Smooth Nonlinear Fitting Scheme for Analog Multiplierless Implementation of Hindmarsh-Rose Neuron Model

Jianming Cai
Changzhou University
Han Bao
Changzhou University
Quan Xu
Changzhou University
Zhongyun Hua
Harbin Institute of Technology Shenzhen
Bocheng Bao (mervinbao@126.com)
Changzhou University https://orcid.org/0000-0001-6413-3038

Research Article

Keywords: Circuit implementation, Hindmarsh-Rose (HR) neuron model, multiplier, nonlinear fitting, nonlinearity

Posted Date: March 9th, 2021

DOI: https://doi.org/10.21203/rs.3.rs-242893/v1

Version of Record: A version of this preprint was published at Nonlinear Dynamics on April 21st, 2021.
See the published version at https://doi.org/10.1007/s11071-021-06453-9.

Smooth nonlinear fitting scheme for analog multiplierless implementation of Hindmarsh−Rose neuron model

Jianming Cai · Han Bao · Quan Xu · Zhongyun Hua · Bocheng Bao

Received: * ** 2021 / Accepted: * ** 2021 / Published online: * ** 2021

Abstract The Hindmarsh-Rose (HR) neuron model is built to describe the neuron electrical activities. Due to the polynomial nonlinearities, multipliers are required to implement the HR neuron model in analog. In order to avoid the multipliers, this brief presents a novel smooth nonlinear fitting scheme. We first construct two nonlinear fitting functions using the composite hyperbolic tangent functions and then implement an analog multiplierless circuit for the two-dimensional (2D) or three- dimensional (3D) HR neuron model. To exhibit the nonlinear fitting effects, numerical simulations and hardware experiments for the fitted HR neuron model are provided successively. The results show that the fitted HR neuron model with analog multiplierless circuit can display different operation patterns of resting, periodic spiking, and periodic/chaotic bursting, entirely behaving like the original HR neuron model. The analog multiplierless circuit has the advantage of low implementation cost and thereby it might be suitable for the hardware implementation of large-scale neural networks.

Keywords Circuit implementation · Hindmarsh-Rose (HR) neuron model · multiplier · nonlinear fitting · nonlinearity.

B. C. Bao (Author for correspondence)
School of Information Science and Engineering, Changzhou University, Changzhou 213164, China
e-mail: mervinbao@126.com

J. M. Cai, H. Bao, and Q. Xu
School of Information Science and Engineering, Changzhou University, Changzhou 213164, China

Z. Y. Hua
School of Computer Science and Technology, Harbin Institute of Technology, Shenzhen, Shenzhen 518055, China

1. Introduction

Neuron, as an essential element of neural network, can exhibit diverse electrical activities in response to the externally imposed stimuli [1–3]. To imitate the biological neuronal dynamics, different mathematical neuron models were presented, including the Hodgkin-Huxley model [4–6], two-dimensional (2D) and three-dimensional (3D) Hindmarsh-Rose (HR) models [7, 8], memristive HR model with threshold electromagnetic induction [9], fractional-order HR model [10], modified Izhikevich model [11], Morris-Lecar model [12, 13], FitzHugh-Nagumo photosensitive model [14], and excitable map-based model [15]. Besides, to develop brain-like hardware devices, different electronic neurons were also developed [16–18]. These neuron models and electronic neurons are extremely useful for keeping the intrinsic mechanisms and bifurcation behaviors of neurons [19], and thus can effectively promote the applications in artificial neural networks [20].

Circuit implementations of mathematical neuron models and large-scale neural networks on a hardware level have received much attention recently [21]. Based on the off-the-shelf analog components and on-chip digital devices, numerous analog and digital neuromorphic circuits were developed to simulate standalone neurons and coupled neural networks [22, 23]. Due to the power-efficiency and compactness of analog circuits, mathematical neuron models were widely implemented in analog [24–26]. Based on numerous off-the-shelf discrete components, Bao et al optimized an analog circuit design to implement an adapting synapse-based neuron model [24], Behdad et al presented an experimental electronic neuron to achieve a complete Morris-Lecar model [25], and Arthur and Boahen developed a silicon-based integrate-and-fire neuron using a dynamical system approach [26].

However, when complex nonlinearities are involved, hardware circuit implementations for mathematical neuron models become extremely difficult. To solve this issue, a large number of digitally FPGA-based piecewise liner approximation approaches were proposed to implement neuromorphic circuits without multipliers [27–33]. Using the digital multiplierless implementation method, Jokar and Soleimani aimed at a calcium-based plasticity model [27], Gomar and Ahmadi focused on a biological adaptive-exponential neuron model [28], and Hayati et al sighted a two-coupled biological HR neuron model [29]. Meanwhile, Rahimian et al implemented a two-compartmental Pinsky-Rinzel pyramidal neuron model in digital [30], Imani et al investigated the multiplierless realization of a coupled Wilson neuron model in digital [32], and Haghiri et al employed a low-cost digital design to implement the noisy Izhikevich neuron model without multipliers [33].

These electronic neurons with analog and digital circuit implementations are capable to reproduce lots of different neuron dynamics and spiking/bursting behaviors that might appear in biological neurons [25, 31]. Encouraged by the above piecewise liner approximation approaches, this paper presents a novel smooth nonlinear fitting scheme to implement an analog multiplierless circuit for the 2D/3D HR neuron model. Using this smooth nonlinear fitting scheme, the polynomial nonlinearities in the 2D/3D HR neuron model can be perfectly fitted by the composite hyperbolic tangent functions. Therefore, the presented smooth nonlinear fitting scheme is suitable for implementing electronic neurons in analog and the designed nonlinear fitting functions are smooth and continuously differentiable. By contrast, the piecewise liner approximation approaches reported in [27–33] are applied by the digitally FPGA-based electronic neurons, and the utilized piecewise linear functions are non-smooth and continuously non-differentiable.

The contributions of this paper are summarized as follows. (1) A novel smooth nonlinear fitting scheme is presented to multiplierlessly implement the 2D/3D HR neuron model and different neuron dynamics and spiking/bursting behaviors are reproduced. (2) An analog multiplierless circuit for the 2D/3D HR neuron model is designed and fabricated on a printed circuit board (PCB). Hardware experiments show that the analog multiplierless circuit can perfectly generate different operation patterns, such as the resting pattern, periodic/chaotic bursting patterns, and periodic spiking patterns with different oscillating frequencies.

The rest of this paper is organized as follows. Section 2 presents a smooth nonlinear fitting scheme and constructs two nonlinear fitting functions for the HR neuron model. Section 3 designs the circuit modules of the smooth nonlinear fitting functions and

develops a hardware device for the analog multiplierless circuit. Finally, this paper is briefly concluded in Section 4.

2. Nonlinear fitting scheme for the HR neuron model

This section presents a smooth nonlinear fitting scheme to implement two polynomial nonlinearities in the HR neuron model.

2.1 Brief descriptions for the HR neuron model

Simplified from the Hodgkin-Huxley neuron model [4], the 2D HR neuron model was firstly introduced in 1982 [7], and it is described as

$$\begin{cases} \dot{x} = y - ax^3 + bx^2 + I, \\ \dot{y} = c - dx^2 - y, \end{cases} \tag{1}$$

where x, y, and I represent the membrane potential, spiking variable, and steady current, respectively.

To exhibit the rich electrical activities of neuronal membrane potential, the 3D HR neuron model was then introduced [8] and it is expressed as

$$\begin{cases} \dot{x} = y - ax^3 + bx^2 + I - z, \\ \dot{y} = c - dx^2 - y, \\ \dot{z} = r(s(x + x_1) - z), \end{cases} \tag{2}$$

where z stands for the bursting variable and x_1 represents the resting potential. The extra variable z is coupled into the 2D HR neuron model to regulate the current I. Generally, the model parameters in (1) and (2) are selected as $a = 1$, $b = 3$, $c = 1$, $d = 5$, $x_1 = 1.6$, $s = 4$, and $r = 0.01$ along with an adjustable current I [9]. Note that the parameter r is a small value and it is amplified to facilitate the selection of circuit parameters.

For the sake of simplicity, denote

$$\begin{aligned} F(x) &= x^3 - 3x^2, \\ G(x) &= 5x^2 - 1. \end{aligned} \tag{3}$$

After substituting the aforementioned parameters and the above equations into (1) and (2), the original 2D HR neuron model in (1) can be rewritten as

$$\begin{cases} \dot{x} = -F(x) + y + I, \\ \dot{y} = -G(x) - y, \end{cases} \tag{4}$$

and the original 3D HR neuron model in (2) can be rewritten as

$$\begin{cases} \dot{x} = -F(x) + y - z + I, \\ \dot{y} = -G(x) - y, \\ \dot{z} = 0.04x + 0.064 - 0.01z, \end{cases} \tag{5}$$

Then, the 2D/3D HR neuron model involves two polynomial nonlinearities: the cubic polynomial $F(x)$ and the quadratic polynomial $G(x)$.

2.2 Novel smooth nonlinear fitting scheme

To physically implement the 2D/3D HR neuron model in analog, the multiplier is a basic component for constructing the quadratic and cubic polynomials. However, the analog circuit with multiplier has higher implementation cost than that without multiplier. To reduce the implementation cost of the 2D/3D HR neuron model, we present a smooth nonlinear fitting scheme without any multiplier to implement the polynomial nonlinearities of the 2D/3D HR neuron model.

The hyperbolic tangent function $\tanh(\cdot)$ in mathematics is smooth differentiable and has the upper and lower bounds. It can be easily implemented using some off-the-shelf analog electronic components. In the presented smooth nonlinear fitting scheme, two

composite hyperbolic tangent functions are utilized to fit the two polynomial nonlinearities of the 2D/3D HR neuron model.

Corresponding to the cubic and quadratic polynomials $F(x)$ and $G(x)$ shown in (3), two smooth nonlinear fitting functions $H_1(x)$ and $H_2(x)$ are realized by the composite hyperbolic tangent functions and described as

$$H_1(x) = m_1 \tanh(\kappa_1 x + \delta_1) + m_2 \tanh(\kappa_2 x - \delta_2) - m_3 \tanh(\kappa_3 x - \delta_3) - \delta_{o1}, \tag{6}$$

$$H_2(x) = m_4 \tanh(\kappa_4 x - \delta_4) - m_5 \tanh(\kappa_5 x + \delta_5) + \delta_{o2}, \tag{7}$$

where m_j, κ_j, and δ_j with $j = 1, 2, 3, 4, 5$, as well as δ_{o1} and δ_{o2} are the parameters of the fitting functions $H_1(x)$ and $H_2(x)$, as listed in Table 1. Thus, $H_1(x)$ consists of three hyperbolic tangent functions while $H_2(x)$ contains two.

Fig. 1 shows the matching accuracy between the original functions $F(x)$ and $G(x)$ in the 2D/3D HR neuron model and their smooth nonlinear fitting versions $H_1(x)$ and $H_2(x)$. The dashed curves show the original functions $F(x)$ and $G(x)$ and the solid curves depict the smooth nonlinear fitting functions $H_1(x)$ and $H_2(x)$. As can be seen, the nonlinear fitting functions are basically consistent with the original functions.

Table 1 Parameters of two smooth nonlinear fitting functions

Functions	Parameters	Values
$H_1(x)$	$(m_1, \kappa_1, \delta_1)$	(38.7, 0.7, 1.8)
	$(m_2, \kappa_2, \delta_2)$	(38.7, 0.7, 3.2)
	$(m_3, \kappa_3, \delta_3)$	(6, 0.8, 0.8)
	δ_{o1}	2
$H_2(x)$	$(m_4, \kappa_4, \delta_4)$	(18, 0.98, 1.74)
	$(m_5, \kappa_5, \delta_5)$	(18, 0.98, 1.74)
	δ_{o2}	32.9

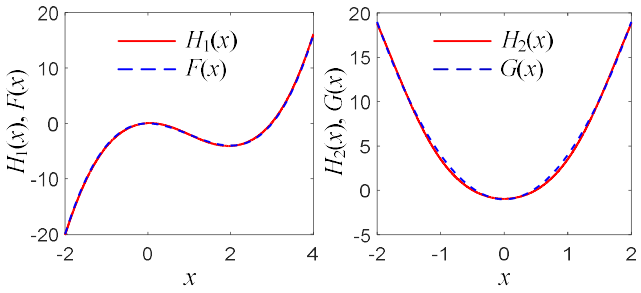

Fig. 1 Two smooth nonlinear fitting functions $H_1(x)$ and $H_2(x)$ for the HR neuron model. The dashed curves represent the original functions $F(x)$ and $G(x)$, and the solid curves represent the nonlinear fitting functions.

It should be stressed that the nonlinear fitting functions $H_1(x)$ and $H_2(x)$ using the presented nonlinear fitting scheme are smooth and continuously differentiable, whereas the piecewise linear approximation functions appeared in [27–33] are non-smooth and continuously non-differentiable.

2.2 Spiking and bursting in the fitted HR neuron model

The classical HR neuron model can show two operation patterns, namely the spiking and bursting. In the spiking pattern, the slow variable z is set as zero and the corresponding system is reduced to a 2D HR neuron model. In this way, the oscillating frequency is closely related to the steady current I. By contrast, in the bursting pattern, the slow variable z is what generates the bursting patterns. Correspondingly, the system is described by a 3D HR neuron model and its operation patterns have the mode transitions from resting to periodic bursting, to chaotic bursting, and finally to spiking patterns as the steady current I increases successively.

To demonstrate the feasibility of the presented smooth nonlinear fitting scheme, we introduce the two fitting functions $H_1(x)$ and $H_2(x)$ into the 2D/3D HR neuron model to replace the original nonlinear functions $F(x)$ and $G(x)$. Thus, the fitted 2D/3D HR neuron model is coined. To exhibit the nonlinear fitting effects, several representative values of the steady current I are selected for the original and fitted 2D/3D HR neuron models.

When the steady current is set as $I = 0.5$ and 2, respectively, the original and fitted 2D HR neuron models operate in the spiking patterns with different oscillating frequencies, and their membrane potentials are shown in Figs. 2a, b. As can be observed, the oscillating frequency increases as the steady current increases. Meanwhile, the two spiking patterns generated by the original and fitted 2D HR neuron models are basically consistent.

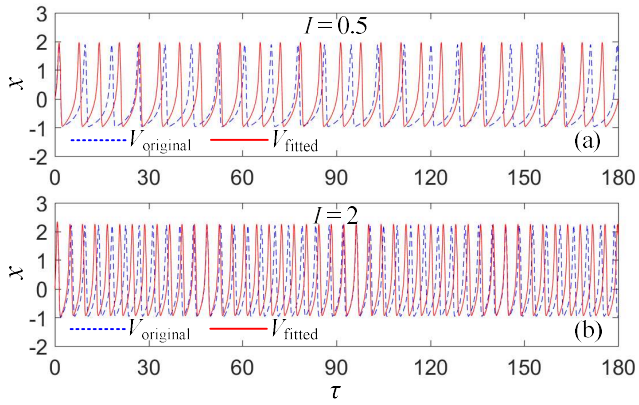

Fig. 2 Operation patterns in the original and fitted 2D HR neuron models for two representative values of I. **a** $I = 0.5$. **b** $I = 2$. The dashed and solid trajectories represent the membrane potentials of the original and fitted 2D HR neuron models respectively.

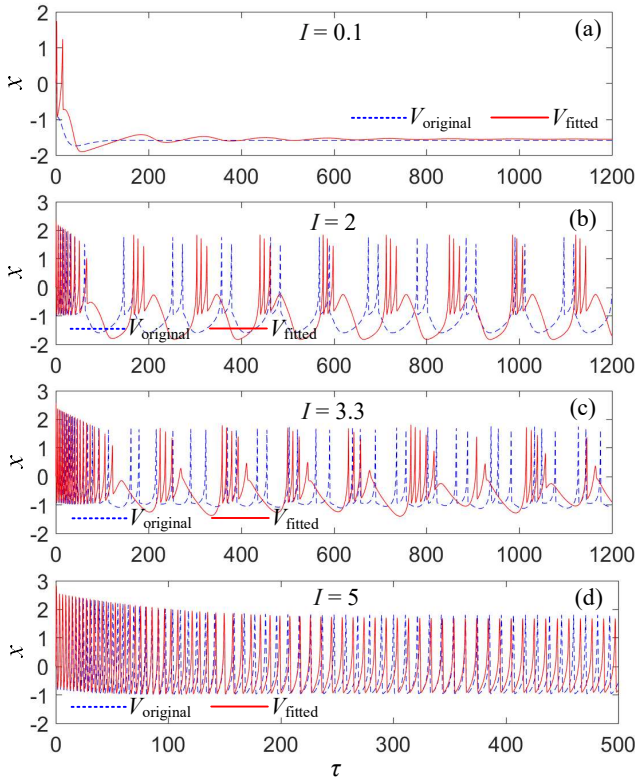

Fig. 3 Operation patterns in the original and fitted 3D HR neuron models for four representative values of I. **a** Resting at $I = 0.1$. **b** Periodic bursting at $I = 2$. **c** Chaotic bursting at $I = 3.3$. **d** Periodic spiking at $I = 5$. The dashed and solid trajectories represent the membrane potentials of the original and fitted 3D HR neuron model, respectively.

For different values of the steady current I, the 3D HR neuron model shows different operation patterns. The four representative values of the steady current are considered as I = 0.1, 2, 3.3, and 5, respectively. When imposing these steady currents on the original and fitted 3D HR neuron models, the membrane potentials can be induced and illustrated in Fig. 3. As can be seen, with the increasement of the steady current, the operation patterns undergo the resting, periodic bursting, chaotic bursting, and periodic spiking patterns sequentially. In the bursting patterns, the busters of the original and fitted 3D HR neuron models have slight difference but their dynamical behaviors are the same. As a result, the fitted 3D HR neuron model can be used to simulate the rich electrical activities of the original 3D HR neuron model, indicating the feasibility of the presented smooth nonlinear fitting scheme.

Since the original and fitted 2D HR neuron models only have the simple periodic spiking dynamics, we take the original and fitted 3D HR neuron models as examples for comparing their bursting dynamics and pattern transitions. Based on the inter-spike interval (ISI), we study the bifurcation diagrams of neuronal membrane potential x with the increment of steady current I. The bifurcation diagrams are plotted by computing the ISI of action spike value of membrane potential x [34] and the numerical results are shown in Fig. 4. When the steady current I increases within the interval [0, 5], both the original and fitted 3D HR neuron models have similar bursting dynamics, and their firing patterns undergo complex mode transitions from the resting, first to periodic bursting, then to chaotic bursting, and finally to periodic spiking patterns. The numerical results manifest that the fitted 3D HR neuron model can perfectly reproduce the complex bursting dynamics and pattern transitions appearing in the original 3D HR neuron model, but their parameter-dependent bifurcation structures are somewhat different. Nevertheless, the numerical results in Fig. 4 further show that the presented smooth nonlinear fitting scheme is feasible.

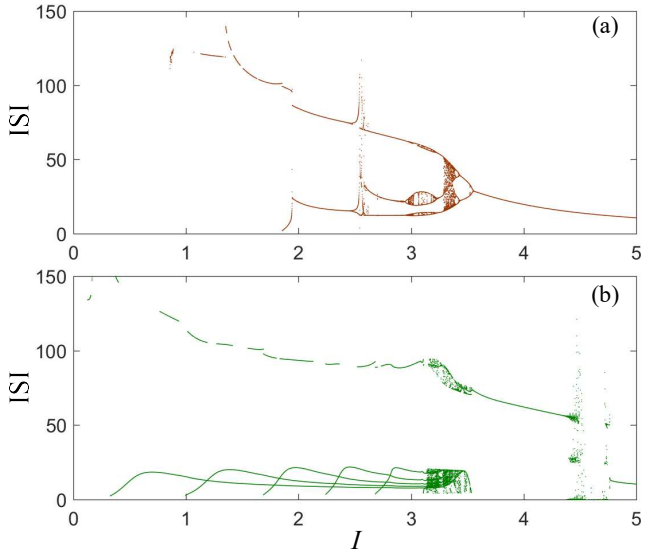

Fig. 4 The ISI-based bifurcation diagrams of neuronal membrane potential x with the increment of steady current I. **a** The original 3D HR neuron model. **b** The fitted 3D HR neuron model.

3. Analog multiplierless circuit design and hardware experiment

This section designs an analog multiplierless circuit of the fitted 2D/3D HR neuron model using the circuit modules of composite hyperbolic tangent functions. Thereafter, a hardware device is developed for the analog multiplierless circuit.

3.1 Analog Multiplierless circuit design

The circuit modules for positive and negative hyperbolic tangent functions were designed in [24, 35], as shown in Figs. 5a, b. They are designed using some off-the-shelf analog components, including operational amplifiers, voltage sources, transistors, and resistors. Note that the current source I_0 is implemented using two transistors, three resistors, and one voltage source [35], and its value is achieved by adjusting a resistance.

For the circuit modules of positive and negative hyperbolic tangent functions in Figs. 5a, b, their transfer characteristics of input voltage v_i and output voltage v_o are described as

$$\begin{aligned} v_o &= \tanh(\kappa v_i \pm \mu E), \\ v_o &= -\tanh(\kappa v_i \pm \mu E), \end{aligned} \tag{8}$$

respectively, where E is a fixed offset voltage, $\mu E = \delta_j$, $\kappa = R_F/(2RV_T)$, and $\mu = R_F/(2R_E V_T) = \kappa R/R_E$. In our design, the offset voltage is connected to the inverting input terminal of the operational amplifier via an adjustable resistor. The intent is to easily achieve different offset values of the hyperbolic tangent function by adjusting the resistance R_E. However, when realizing the offset values of the hyperbolic tangent function, the offset voltage connection method reported in the literature [24, 35] should adjust the offset voltage. This requires the power supply to provide multiple and high precision DC voltage outputs, and thus greatly increases the difficulty of hardware circuit experiment. In short, the circuit modules of positive and negative hyperbolic tangent functions in Figs. 5a, b are designed optimally in this paper.

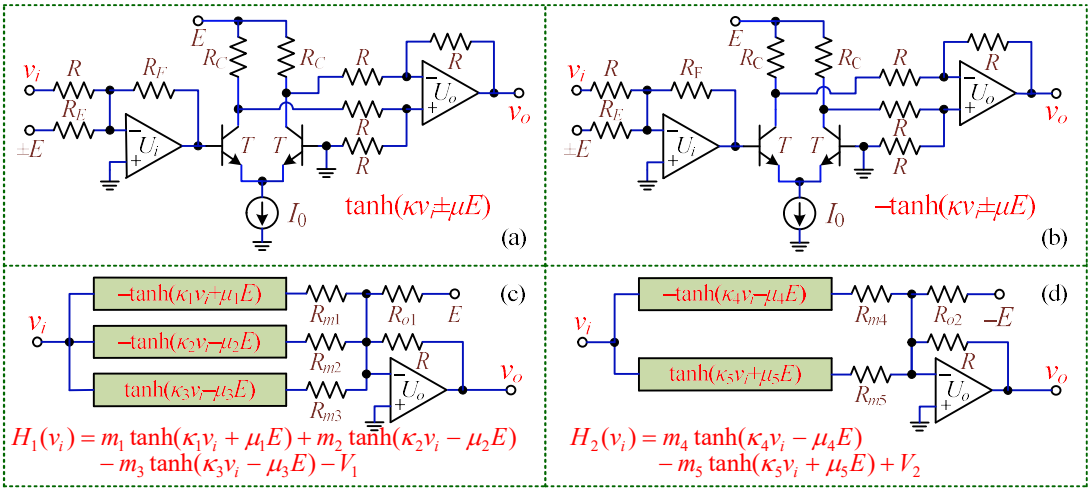

Fig. 5 Circuit implementations for two nonlinear fitting functions $H_1(x)$ and $H_2(x)$. **a** Circuit module for tanh(·) with an offset voltage. **b** Circuit module for −tanh(·) with an offset voltage. **c** Circuit module for $H_1(x)$. **d** Circuit module for $H_2(x)$.

Table 2 Desired resistances for two nonlinear fitting functions

Functions	Resistances	Values (kΩ)
$v_o = H_1(v_i)$	(R_{m1}, R_{F1}, R_{E1})	(0.258, 0.364, 58.333)
	(R_{m2}, R_{F2}, R_{E2})	(0.258, 0.364, 32.813)
	(R_{m3}, R_{F3}, R_{E3})	(1.667, 0.416, 150.00)
	R_{o1}	75.000
$v_o = H_2(v_i)$	(R_{m4}, R_{F4}, R_{E4})	(0.556, 0.510, 84.483)
	(R_{m5}, R_{F5}, R_{E5})	(0.556, 0.510, 84.483)
	R_{o2}	4.559

With these circuit modules of hyperbolic tangent functions shown in Figs. 5a, b, two nonlinear fitting functions $H_1(x)$ and $H_2(x)$ given in (6) and (7) can be directly designed and their circuit modules are shown in Figs. 5c, d, respectively. When applying an input v_i, the outputs of the two circuit modules in Figs. 5c, d can be represented as

$$H_1(v_i) = m_1 \tanh(\kappa_1 v_i + \mu_1 E) + m_2 \tanh(\kappa_2 v_i - \mu_2 E) - m_3 \tanh(\kappa_3 v_i - \mu_3 E) - V_1, \tag{9}$$

$$H_2(v_i) = m_4 \tanh(\kappa_4 v_i - \mu_4 E) - m_5 \tanh(\kappa_5 v_i + \mu_5 E) + V_2, \tag{10}$$

where $m_j = R/R_{mj}$ with j = 1, 2, 3, 4, 5, $V_1 = \delta_{o1} = RE/R_{o1}$, and $V_2 = \delta_{o2} = RE/R_{o2}$.

The circuit parameters R = 10 kΩ, R_C = 1 kΩ, E = 15 V, I_0 = 1.3 mA, and V_T = 26 mV are determined. Using the parameter settings of the nonlinear fitting functions $H_1(x)$ and $H_2(x)$ shown in Table 1, the desired resistances of all circuit modules in Fig. 5 can be calculated and listed in Table 2. Thus, the cubic and quadratic polynomials $F(x)$ and $G(x)$ given in (3) can be approximately achieved using relatively cheap commercial electronic components.

Using the two circuit modules shown in Figs. 5c, d, the analog multiplierless implementation circuit of the fitted 2D/3D HR neuron model can be designed and drawn in Fig. 6. The upper part is two integral channels with the circuit modules of $H_1(v_x)$ and $H_2(v_x)$, and the lower part is an extra integral channel for implementing the slow variable v_z. Based on three capacitor voltages v_x, v_y, and v_z in Fig. 6, the circuit state equations under the physical time $t = RC\tau$ are established as

$$\begin{aligned} RC\frac{\mathrm{d}v_x}{\mathrm{d}t} &= -H_1(v_x) + v_y - v_z + \frac{R}{R_I}E, \\ RC\frac{\mathrm{d}v_y}{\mathrm{d}t} &= -H_2(v_x) - v_y, \\ RC\frac{\mathrm{d}v_z}{\mathrm{d}t} &= 0.04v_x + 0.0043E - 0.01v_z, \end{aligned} \tag{11}$$

where R_I is a resistance to adjust the steady current.

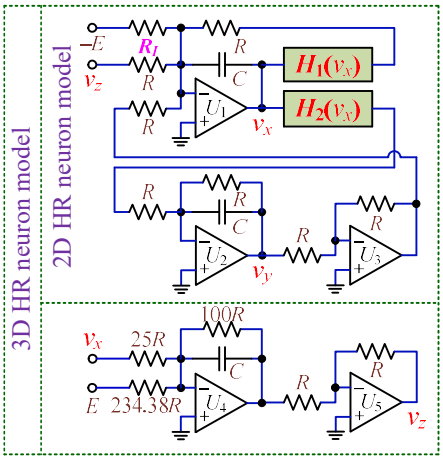

Fig. 6 Analog multiplierless implementation of the fitted 2D/3D HR neuron model.

Compared (11) with (5), the resistance R_I for adjusting the steady current I can be expressed as

$$R_I = \frac{RE}{I}. \tag{12}$$

Thus, different spiking and bursting patterns can be displayed from the designed analog multiplierless circuit by adjusting the resistance R_I achieved by a precise potentiometer.

3.2 PCB-based hardware experiments

Based on the circuit schematics shown in Figs. 5 and 6, a hardware device for the analog multiplierless circuit of the fitted 2D/3D HR neuron model is welded on a PCB level. Fig. 7 shows a picture of the hardware device. Here, the resistors, capacitors, precise potentiometers, MPS2222 transistors, and TL082CP operational amplifiers are employed. The off-the-peg ±15 V DC power module is used to provide the supply voltages of the operational amplifiers and offset voltages of the circuit modules. The experimental outputs are captured by the WaveSurfer 510 oscilloscope. Due to the limitation of saturation output level, it is necessary to ensure that the operational amplifier supplied by ±15 V DC power module operates within a linear operating range

about ±13 V. In addition, I_0 can be adjusted by a specific potentiometer and one can refer to [35] for more details.

Fig. 8 shows the screenshots of the hardware experimental prototype with the captured transfer characteristic curve for the circuit module $H_1(v_i)$ and periodic bursting pattern for the fitted 3D HR neuron model.

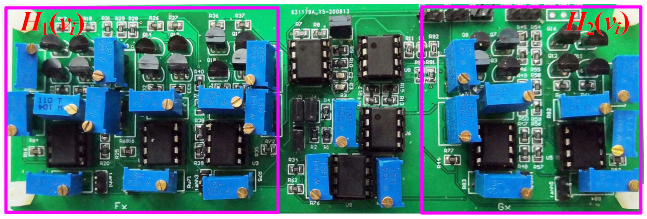

Fig. 7 The PCB-based hardware device for the analog multiplierless circuit of the fitted 2D/3D HR neuron model. The two circuit modules of $H_1(v_i)$ and $H_2(v_i)$ are located in the left and right line boxes respectively.

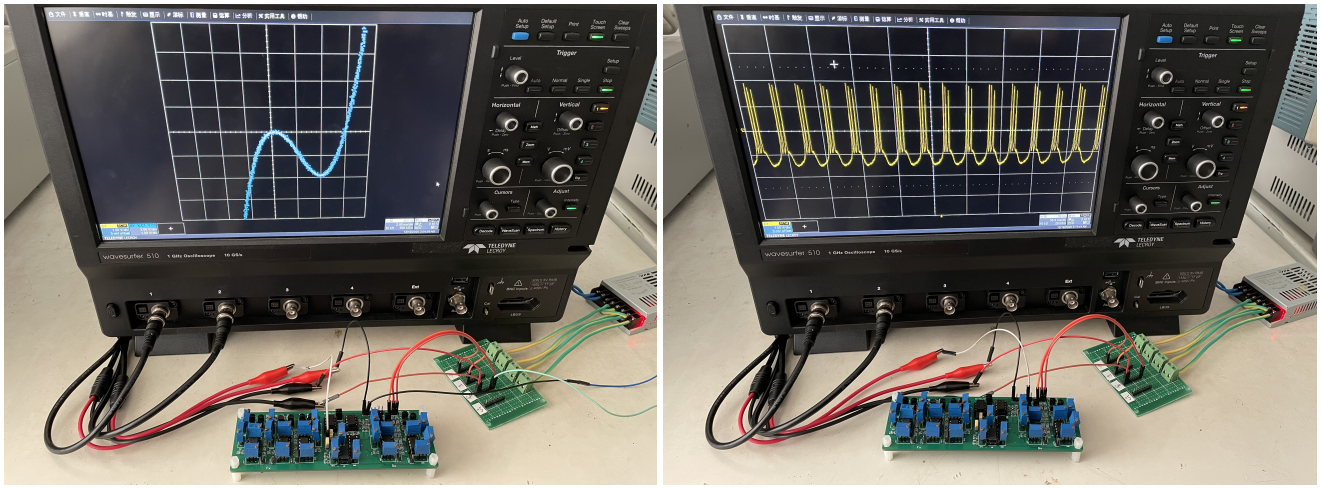

Fig. 8 Hardware experimental prototype with the captured transfer characteristic curve for the circuit module $H_1(v_i)$ (left) and periodic bursting pattern for the fitted 3D HR neuron model (right).

When taking the scanning AC voltage $v_i = 6\sin(200\pi t)$ V as the inputs of the two circuit modules $H_1(v_i)$ and $H_2(v_i)$, the transfer characteristic curves in the $v_i - v_o$ voltage plane are measured and shown in Fig. 9. The experimental measurements are consistent with the numerical simulations given in Fig. 1, manifesting the feasibility of the presented smooth nonlinear fitting scheme in the analog circuit implementation.

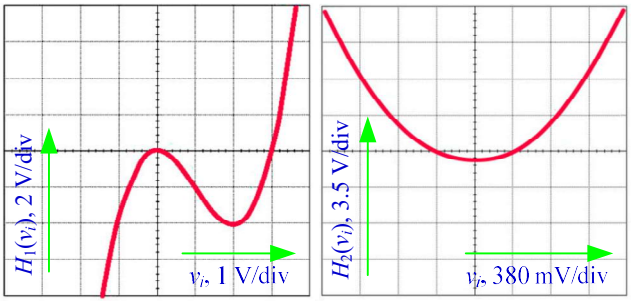

Fig. 9 The experimentally measured transfer characteristic curves in the $v_i - v_o$ voltage plane for the two circuit modules $H_1(v_i)$ and $H_2(v_i)$.

Following the relation in (12), the resistance R_I is employed for adjusting the values of the steady current I. First, disconnect the jumper and select the implementation circuit of the fitted 2D HR neuron model. Corresponding to Fig. 2, the spiking patterns for two representative values of R_I are measured and shown in Fig. 10. Next, connect the jumper and select the analog implementation

circuit of the fitted 3D HR neuron model. Corresponding to Fig. 3, the resting, periodic/chaotic bursting, and periodic spiking patterns for the four representative values of I are measured, as shown in Fig. 11. Consequently, various electrical activities can also be acquired from the analog multiplierless circuit of the fitted 2D/3D HR neuron model as well. The hardware experiments show that the presented smooth nonlinear fitting scheme can implement the 2D/3D HR neuron model without any multiplier.

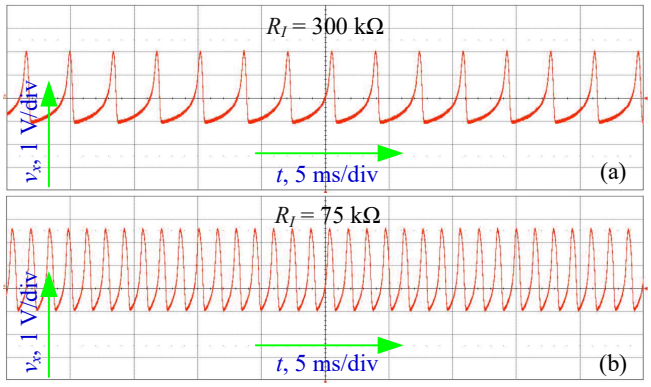

Fig. 10 The experimentally measured spiking patterns in the fitted 2D HR neuron model for two representative values of R_I. **a** R_I = 300 kΩ and **b** R_I = 75 kΩ.

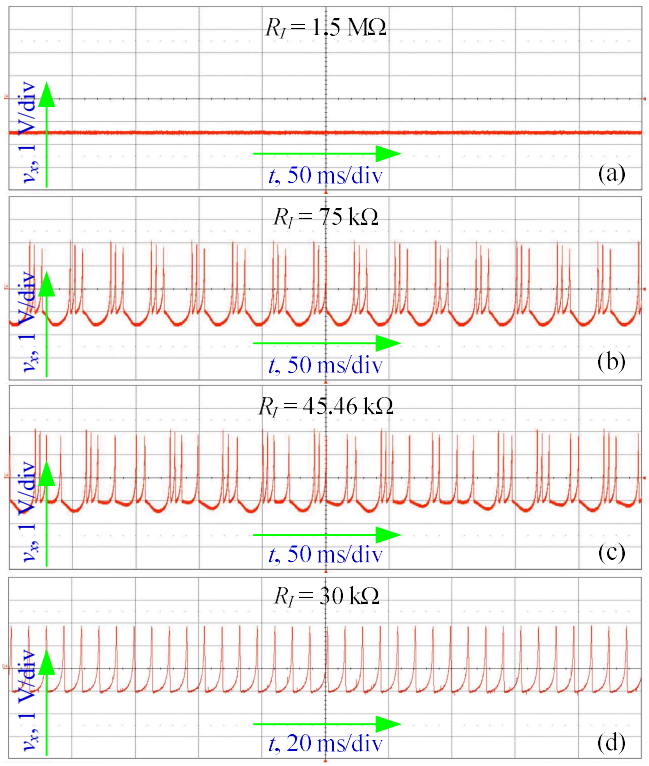

Fig. 11 The experimentally measured operation patterns in the fitted 3D HR neuron model for four representative values of R_I. **a** Resting at R_I = 1.5 MΩ, **b** periodic bursting at R_I = 75 kΩ, **c** chaotic bursting at R_I = 45.46 kΩ, and **d** periodic spiking at R_I = 30 kΩ.

In the hardware experiments, only the resistances in the circuit modules $H_1(v_i)$ and $H_2(v_i)$ need to be fine-tuned. Corresponding to the desired resistances listed in Table 2, the measured resistances are determined by Precision LCR Meter and listed in Table 3. By comparing the values in Tables 2 and 3, one can see that the measured and desired resistances have some slight deviations. These slight deviations are caused by the model idealizations, parasitic parameters, measurement errors, and so on.

The Mean Absolute Percentage Error (MAPE) introduced in [36] can be used to evaluate the deviations between the measured

and desired resistances. Denote $R_{\text{desired}k}$ as the desired value in Table 2 and $R_{\text{measured}k}$ as the measured value in Table 3. The MAPE in the hardware experiments is described by

$$\text{MAPE} = \frac{1}{N}\sum_{k=1}^{N}\frac{\left|R_{\text{desired}k} - R_{\text{measured}k}\right|}{R_{\text{desired}k}} \times 100\%, \tag{13}$$

where N represents the number of resistance samples. According to the values listed in Tables 2 and 3, we can obtain that $N = 17$ and MAPE = 2.4% and this evaluation result is an acceptable precision for the PCB-based hardware experiments.

Table 3 Measured resistances for two nonlinear fitting functions

Functions	Resistances	Values (kΩ)
$v_o = H_1(v_i)$	(R_{m1}, R_{F1}, R_{E1})	(0.244, 0.378, 54.069)
	(R_{m2}, R_{F2}, R_{E2})	(0.257, 0.375, 31.187)
	(R_{m3}, R_{F3}, R_{E3})	(1.667, 0.425, 150.00)
	R_{o1}	75.036
$v_o = H_2(v_i)$	(R_{m4}, R_{F4}, R_{E4})	(0.554, 0.502, 87.356)
	(R_{m5}, R_{F5}, R_{E5})	(0.560, 0.506, 88.781)
	R_{o2}	4.440

4. Conclusions

In this paper, we presented a smooth nonlinear fitting scheme for the 2D/3D HR neuron model. When implementing an analog circuit, the presented smooth nonlinear fitting scheme can avoid multipliers by employing two nonlinear fitting functions. Therefore, without any multiplier, the analog circuit has low implementation cost, and thus is suitable for the hardware implementation of large-scale neural networks. Numerical simulations of the fitted 2D/3D HR neuron model and hardware experiments of the analog multiplierless circuit can reproduce various neuronal electrical activities with an acceptable error. Certainly, the presented smooth nonlinear fitting scheme can also be applied in other neuron models or neural networks, such as the Morris-Lecar neuron model [25] and coupled Hindmarsh-Rose neuron model [29], which deserve our future study.

Acknowledgements

This work was supported by the National Natural Science Foundation of China under Grant 51777016, Grant 61801054, and Grant 66207114 and the Natural Science Foundation of Jiangsu Province, China, under Grant BK20191451.

Compliance with ethical standards

Conflict of interest The authors declare that they have no conflicts of interest. These authors contribute equally to this work.

References

1. Ma, J., Tang, J.: A review for dynamics in neuron and neuronal network. Nonlinear Dyn. **89**(3), 1569–1578 (2017)
2. Izhikevich, E. M.: Dynamical Systems in Neuroscience: The Geometry of Excitability and Bursting. Cambridge, MA, USA: MIT Press (2010)
3. Ma, J., Yang, Z. Q., Yang, L. J., Tang, J.: A physical view of computational neurodynamics. J. Zhejiang Univ. Sci. A **20**(9), 639−659 (2019)
4. Hodgkin, A. L., Huxley, A. F.: A quantitative description of membrane current and its application to conduction and excitation in nerve. J. Physiol. **117**(4), 500–544 (1952)
5. Xu, Y., Jia, Y., Ge, M. Y., Lu, L. L., Yang, L. J., Zhan, X.: Effects of ion channel blocks on electrical activity of stochastic Hodgkin-Huxley neural network under electromagnetic induction Neurocomputing **283**, 196–204 (2018)

6. Hu, X., Liu, C.: Dynamic property analysis and circuit implementation of simplified memristive Hodgkin-Huxley neuron model. Nonlinear Dyn. **97**, 1721–1733 (2019)
7. Hindmarsh, J. L., Rose, R. M.: A model of the nerve impulse using two first-order differential equations. Nature. **296**(5853), 162–164 (1982)
8. Hindmarsh, J. L., Rose, R. M.: A model of neuronal bursting using three coupled first order differential equations. Proc. Roy. Soc. London B Biol. Sci. **221**(1222), 87–102 (1984)
9. Bao, H., Hu, A. H., Liu, W. B., Bao, B. C.: Hidden bursting firings and bifurcation mechanisms in memristive neuron model with threshold electromagnetic induction. IEEE Trans. Neural Netw. Learn. Syst. **31**(2), 502–511 (2020)
10. Kaslik, E.: Analysis of two-and three-dimensional fractional-order Hindmarsh-Rose type neuronal models. Fract. Calc. Appl. Anal. **20**(3), 623–645 (2017)
11. Zhang, S., Cui, K., Zhang, X., Shi, X., Ge, M., Zhao, M., Xu, G., Yan, W.: Effect of transcranial ultrasonic–magnetic stimulation on two types of neural firing behaviors in modified Izhikevich model. IEEE Trans. Magnetics. **54**(3), 5000204 (2018)
12. Hu, X., Liu, C., Liu, Ni, J., Li, S.: An electronic implementation for Morris-Lecar neuron model. Nonlinear Dyn. **84**(4), 2317–2332 (2016)
13. Bao, B. C., Yang, Q. F., Zhu, L., Bao, H., Xu, Q., Yu, Y. J., Chen, M.: Chaotic bursting dynamics and coexisting multi-stable firing patterns in 3D autonomous Morris–Lecar model and microcontroller-based validations. Int. J. Bifurcation Chaos **29**(10), 1950134 (2019)
14. Liu, Y., Xu, W.J., Ma, J., Alzahrani, F., Hobiny, A.: A new photosensitive neuron model and its dynamics. Front. Inform. Technol. Electron. Eng. (2020).
15. Girardi-Schappo, M., Tragtenberg, M. H. R., Kinouchi, O.: A brief history of excitable map-based neurons and neural networks. J. Neurosci. Methods. **220**(2), 116–130 (2013)
16. Larras, B., Lahuec, C., Seguin, F., Arzel, M.: Ultra-low-energy mixed-signal IC implementing encoded neural networks. IEEE Trans. Circuits Syst. I, Reg. Papers. **63**(11), 1974–1985 (2016)
17. Jiang, Y. N., Huang, P., Zhu, D.B., Han, R. Z., Liu, L. F., Liu, X. Y., Kang, J. F.: Design and hardware implementation of neuromorphic systems with RRAM synapses and threshold-controlled neurons for pattern recognition. IEEE Trans. Circuits Syst. I, Reg. Papers. **65**(9), 2726–2738 (2018)
18. Ribar, L., Sepulchre, R.: Neuromodulation of neuromorphic circuits. IEEE Trans. Circuits Syst. I, Reg. Papers. **66**(8), 3028–3040 (2019)
19. Bao, H., Liu, W. B., Chen, M.: Hidden extreme multistability and dimensionality reduction analysis for an improved non-autonomous memristive FitzHugh-Nagumo circuit. Nonlinear Dyn. **96**(3), 1879–1894 (2019)
20. Hu, X. F., Feng, G., Duan, S. K., Liu, L.: A memristive multilayer cellular neural network with applications to image processing. IEEE Trans. Neural Netw. Learn. Syst. **28**(8), 1889–1901 (2017)
21. Jokar, E., Abolfathi, H., Ahmadi, A., Ahmadi, M.: An efficient uniform-segmented neuron model for large-scale neuromorphic circuit design: Simulation and FPGA synthesis results. IEEE Trans. Circuits Syst. I, Reg. Papers. **66**(6), 2336–2349 (2019)
22. Jokar, E., Soleimani, H., Drakakis, E. M.: Systematic computation of nonlinear bilateral dynamical systems with a novel low-power logdomain circuit. IEEE Trans. Circuits Syst. I, Reg. Papers. **64**(8), 2013–2025 (2017)
23. Heidarpur, M., Ahmadi, A., Ahmadi, M., Azghadi, M. R.: CORDIC- SNN: On-FPGA STDP learning with Izhikevich neurons. IEEE Trans. Circuits Syst. I, Reg. Papers. **66**(7), 2651–2661 (2019)
24. Bao, B. C., Zhu, Y. X., Li, C. Q., Bao, H., Xu, Q.: Global multistability and analog circuit implementation of an adapting synapse-based neuron model. Nonlinear Dyn. **101**(2), 1105–1118 (2020)
25. Behdad, R., Binczak, S., Dmitrichev, A. S., Nekorkin, V. I., Bilbault, J. M.: Artificial electrical Morris-Lecar neuron. IEEE Trans. Neural Netw. Learn. Syst. **26**(9), 1875–1884 (2015)
26. Arthur, J. V., Boahen, K. A.: Silicon-neuron design: A dynamical systems approach. IEEE Trans. Circuits Syst. I, Reg. Papers. **58**(5), 1034–1043 (2011)
27. Jokar, E., Soleimani, H.: Digital multiplierless realization of a calcium-based plasticity model. IEEE Trans. Circuits Syst. II, Exp. Briefs. **64**(7), 832–836 (2017)
28. Gomar, S., Ahmadi, A.: Digital multiplierless implementation of biological adaptive-exponential neuron model. IEEE Trans. Circuits Syst. I, Reg. Papers. **61**(4), 1206–1219 (2014)

29. Hayati, M., Nouri, M., Abbott, D., Haghiri, S.: Digital multiplierless realization of two-coupled biological Hindmarsh-Rose neuron model. IEEE Trans. Circuits Syst. II, Express Briefs. **63**(5), 463–467 (2016)
30. Rahimian, E., Zabihi, S., Amiri, M., Linares-Barranco, B.: Digital implementation of the two-compartmental Pinsky–Rinzel pyramidal neuron model. IEEE Trans. Biomed. Circuits Syst. **12**(1), 47–57 (2018)
31. Matsuda, C., Torikai, H.: A novel generalized PWC neuron model: Theoretical analyses and efficient design of bifurcation mechanisms of bursting. IEEE Trans. Circuits Syst. II, Express Briefs. **65**(11), 1738–1742 (2018)
32. Imani, M. A., Ahmadi, A., Rad Malekshahi, M., Haghiri, S.: Digital multiplierless realization of coupled Wilson neuron model. IEEE Trans. Biomed. Circuits Syst. **12**(6), 1431–1439 (2018)
33. Haghiri, S., Zahedi, A., Naderi, A., Ahmadi, A.: Multiplierless implementation of noisy Izhikevich neuron with low cost digital design. IEEE Trans. Biomed. Circuits Syst. **12**(6), 1422–1430 (2018)
34. Gu, H. G., Pan, B. B., Chen, G. R., Duan, L. X.: Biological experimental demonstration of bifurcations from bursting to spiking predicted by theoretical models. Nonlinear Dyn. **78**(1), 391–407 (2014)
35. Bao, B. C., Qian, H., Wang, J., Xu, Q., Chen, M., Wu, H. G., Yu, Y. J.: Numerical analyses and experimental validations of coexisting multiple attractors in Hopfield neural network. Nonlinear Dyn. **90**(4), 2359–2369 (2017)
36. De Myttenaere, A., Golden, B., Le Grand, B., Rossi, F.: Mean Absolute Percentage Error for regression models. Neurocomputing, **192**, 38–48 (2016)

Figures

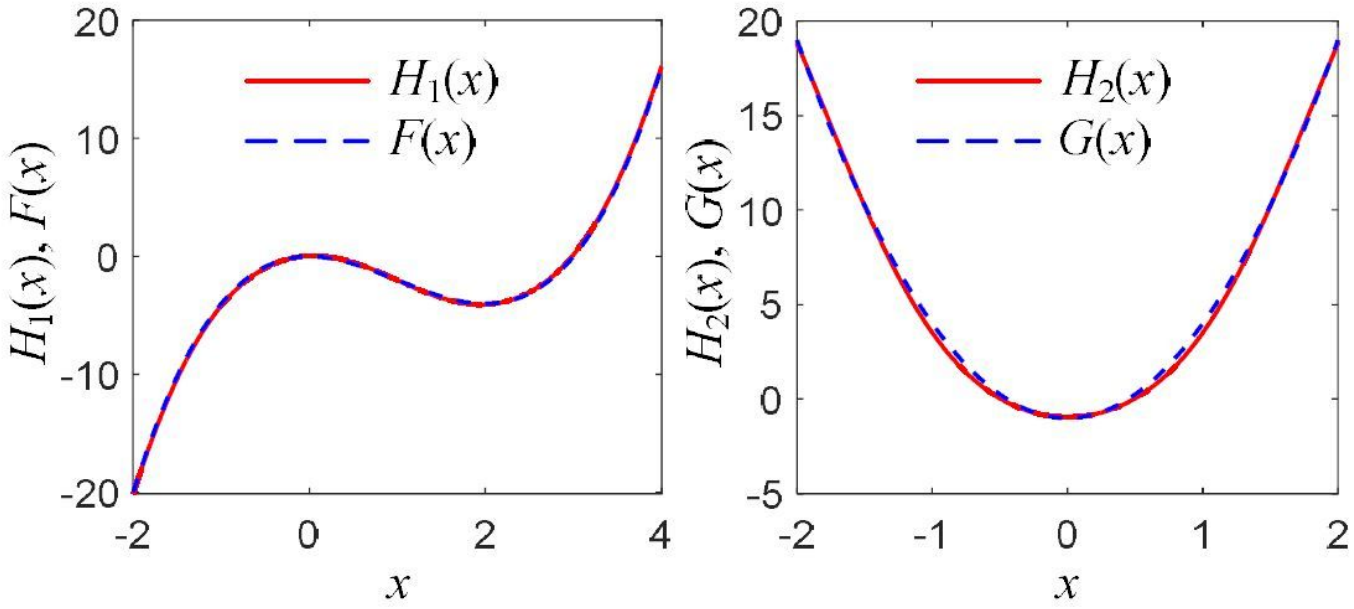

Figure 1

Two smooth nonlinear fitting functions H1(x) and H2(x) for the HR neuron model. The dashed curves represent the original functions F(x) and G(x), and the solid curves represent the nonlinear fitting functions.

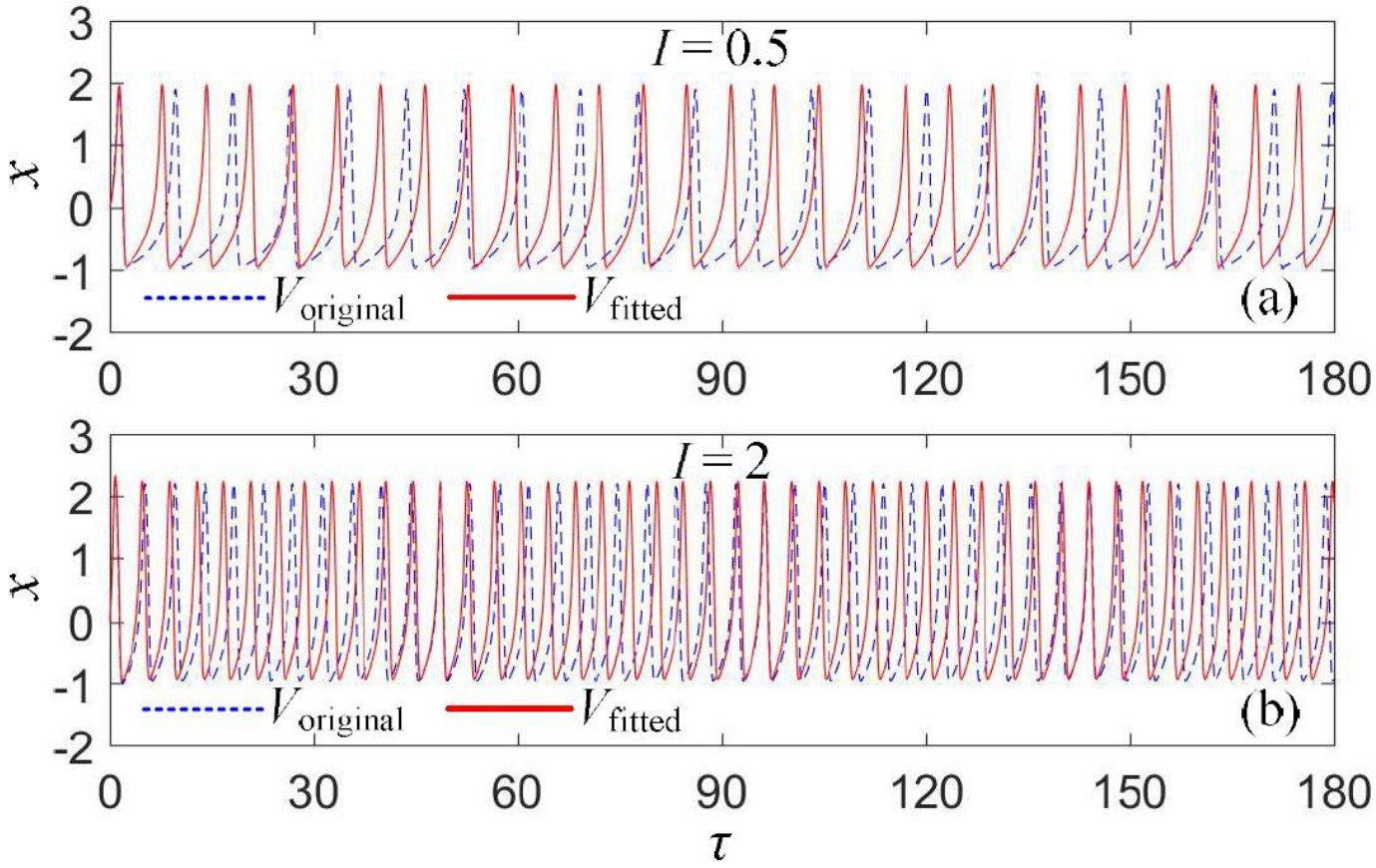

Figure 2

Operation patterns in the original and fitted 2D HR neuron models for two representative values of I. a I = 0.5. b I = 2. The dashed and solid trajectories represent the membrane potentials of the original and fitted 2D HR neuron models respectively.

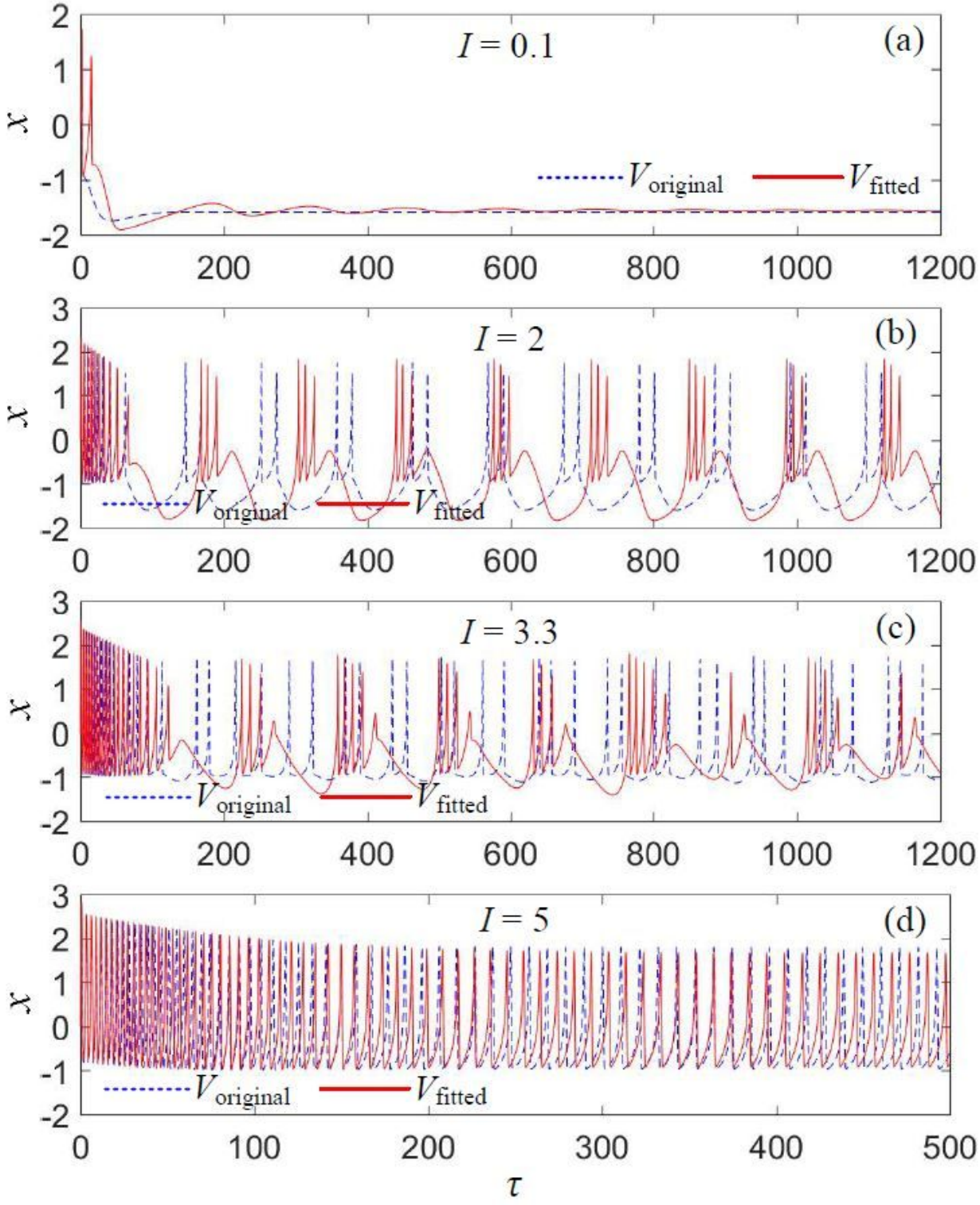

Figure 3

Operation patterns in the original and fitted 3D HR neuron models for four representative values of I. a Resting at I = 0.1. b Periodic bursting at I = 2. c Chaotic bursting at I = 3.3. d Periodic spiking at I = 5. The dashed and solid trajectories represent the membrane potentials of the original and fitted 3D HR neuron model, respectively.

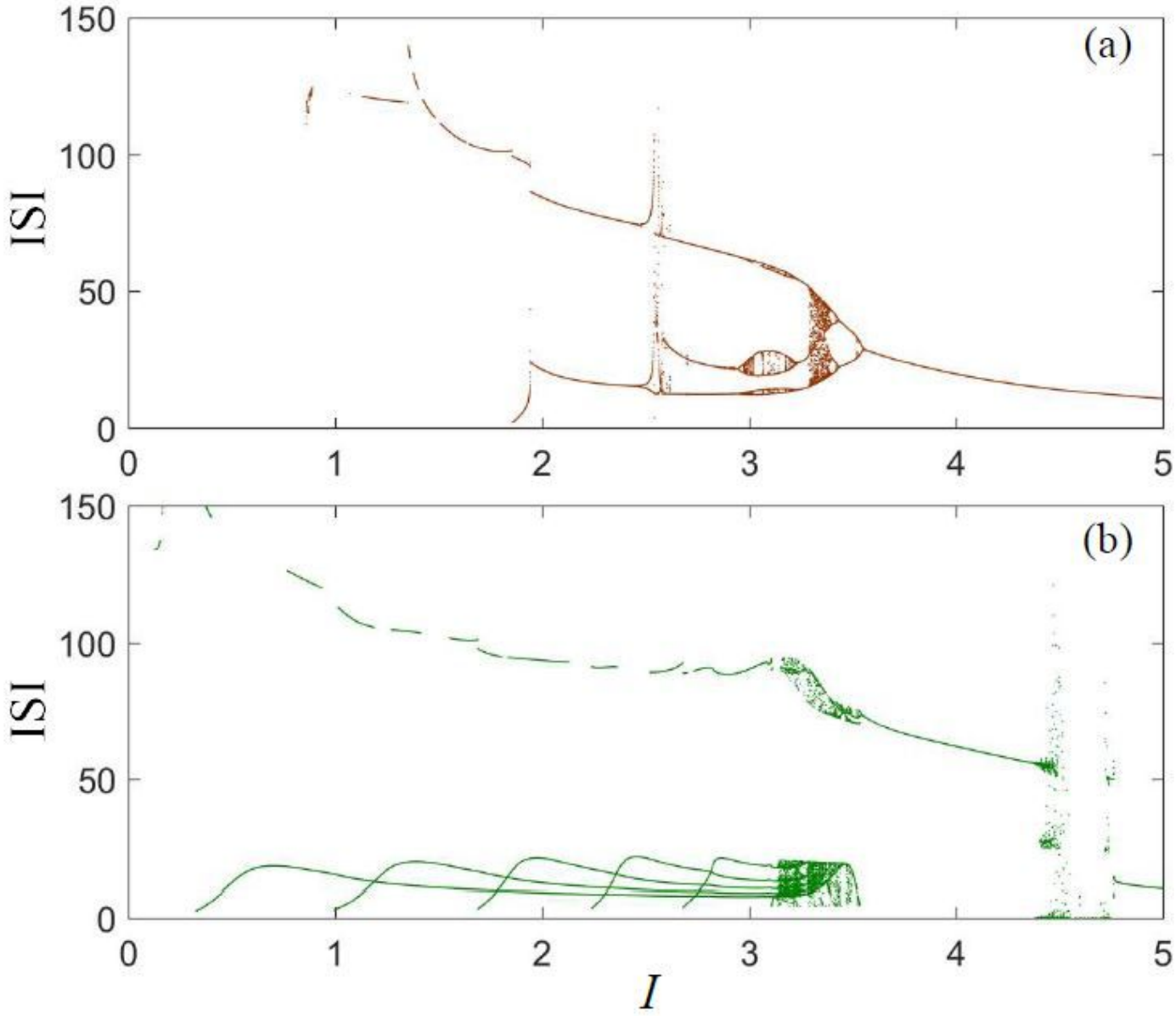

Figure 4

The ISI-based bifurcation diagrams of neuronal membrane potential x with the increment of steady current I. a The original 3D HR neuron model. b The fitted 3D HR neuron model.

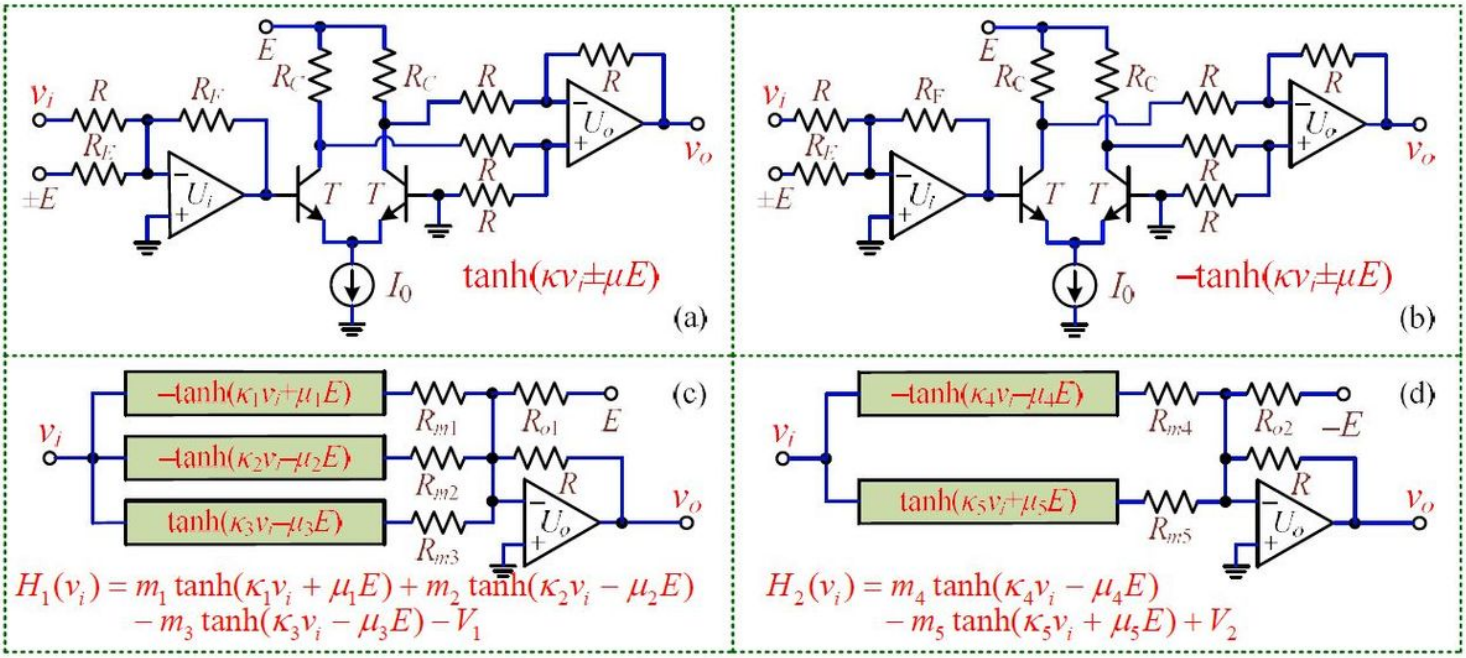

Figure 5

Circuit implementations for two nonlinear fitting functions H1(x) and H2(x). a Circuit module for tanh(□) with an offset voltage. b Circuit module for −tanh(□) with an offset voltage. c Circuit module for H1(x). d Circuit module for H2(x).

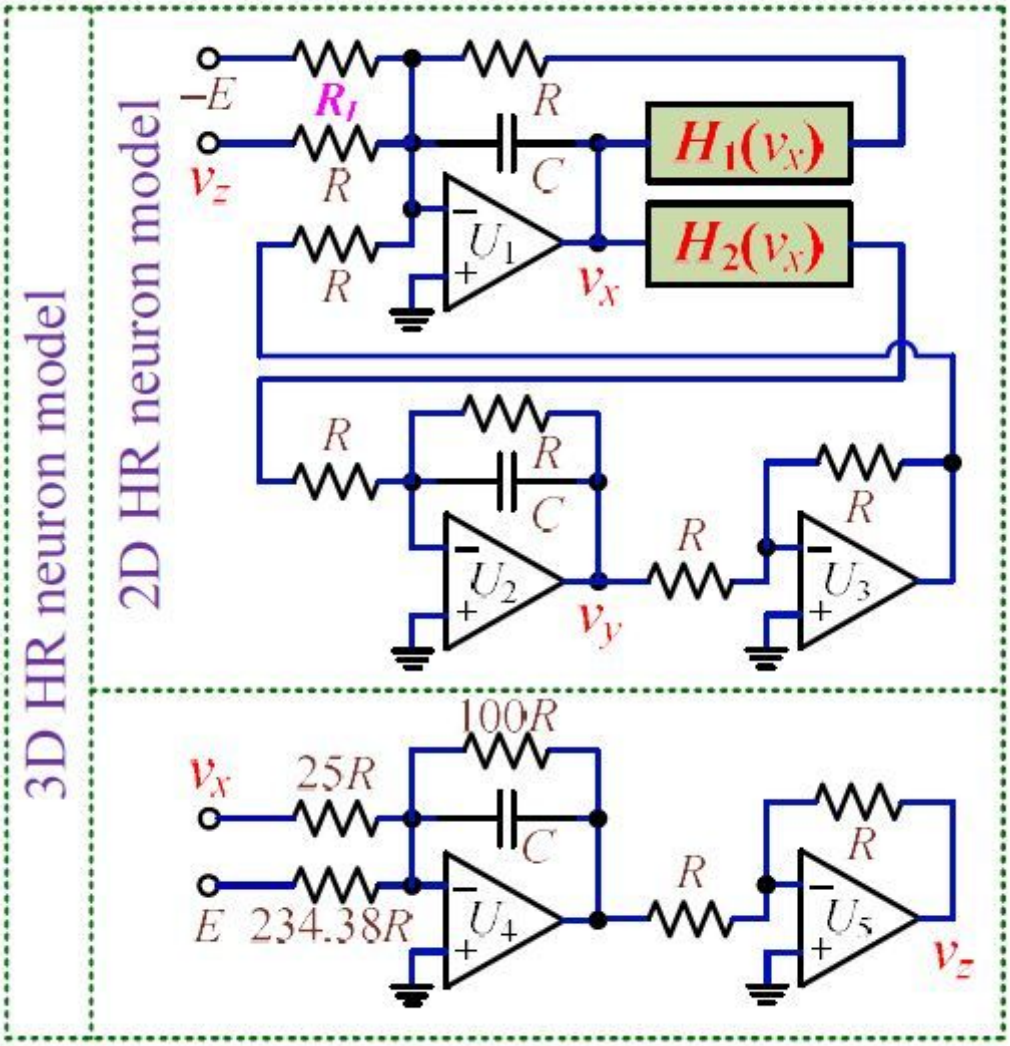

Figure 6

Analog multiplierless implementation of the fitted 2D/3D HR neuron model.

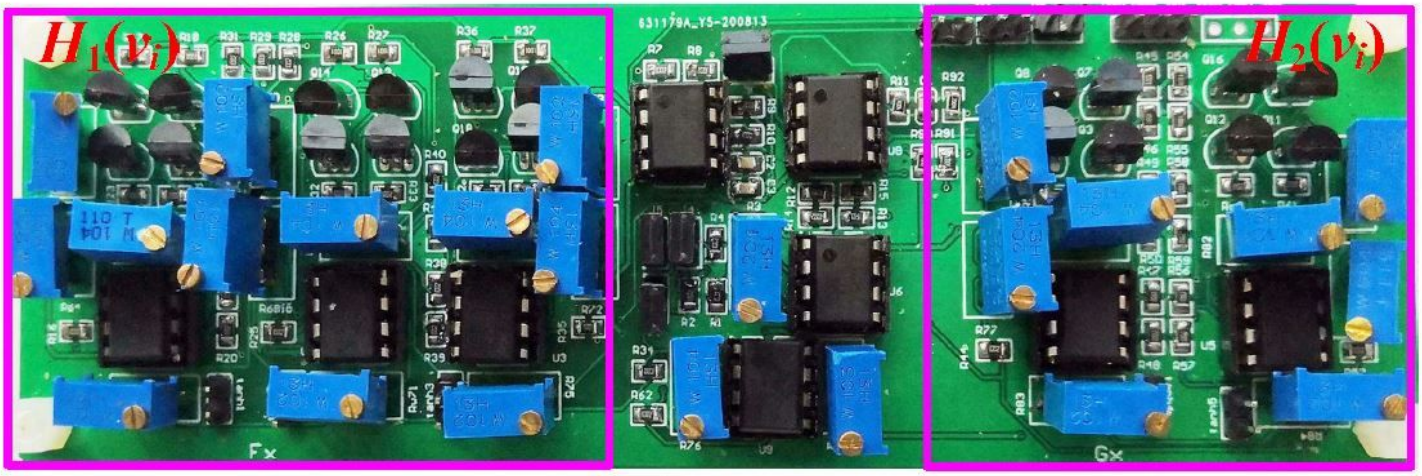

Figure 7

The PCB-based hardware device for the analog multiplierless circuit of the fitted 2D/3D HR neuron model. The two circuit modules of H1(vi) and H2(vi) are located in the left and right line boxes respectively.

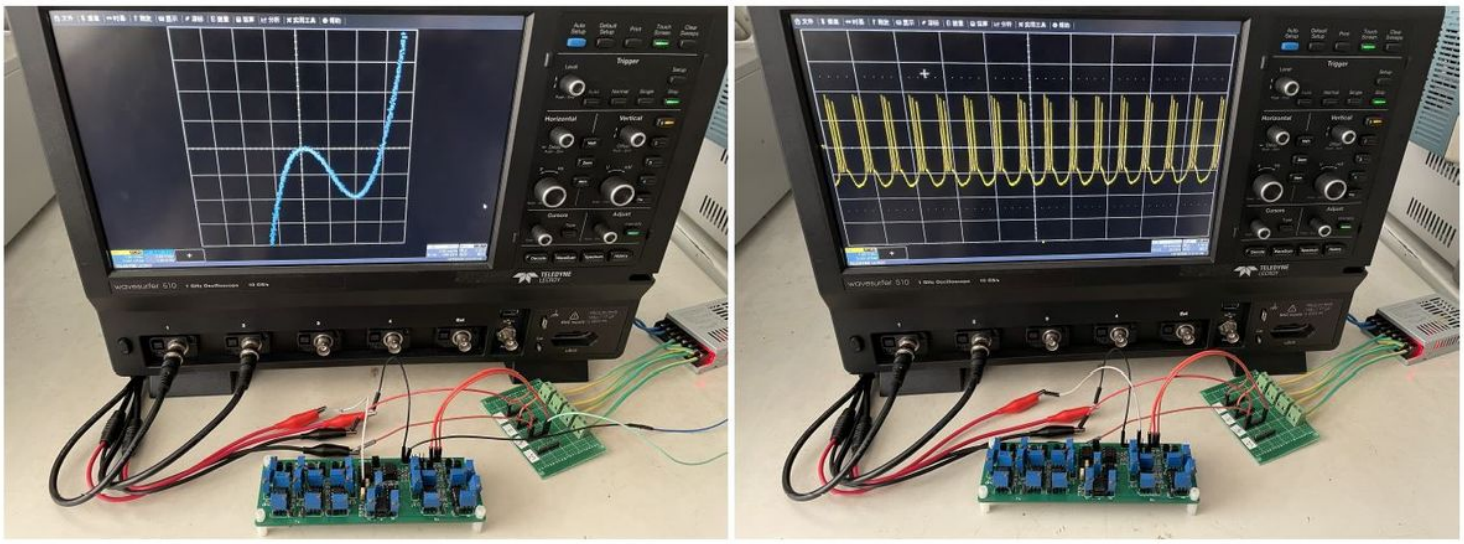

Figure 8

Hardware experimental prototype with the captured transfer characteristic curve for the circuit module H1(vi) (left) and periodic bursting pattern for the fitted 3D HR neuron model (right).

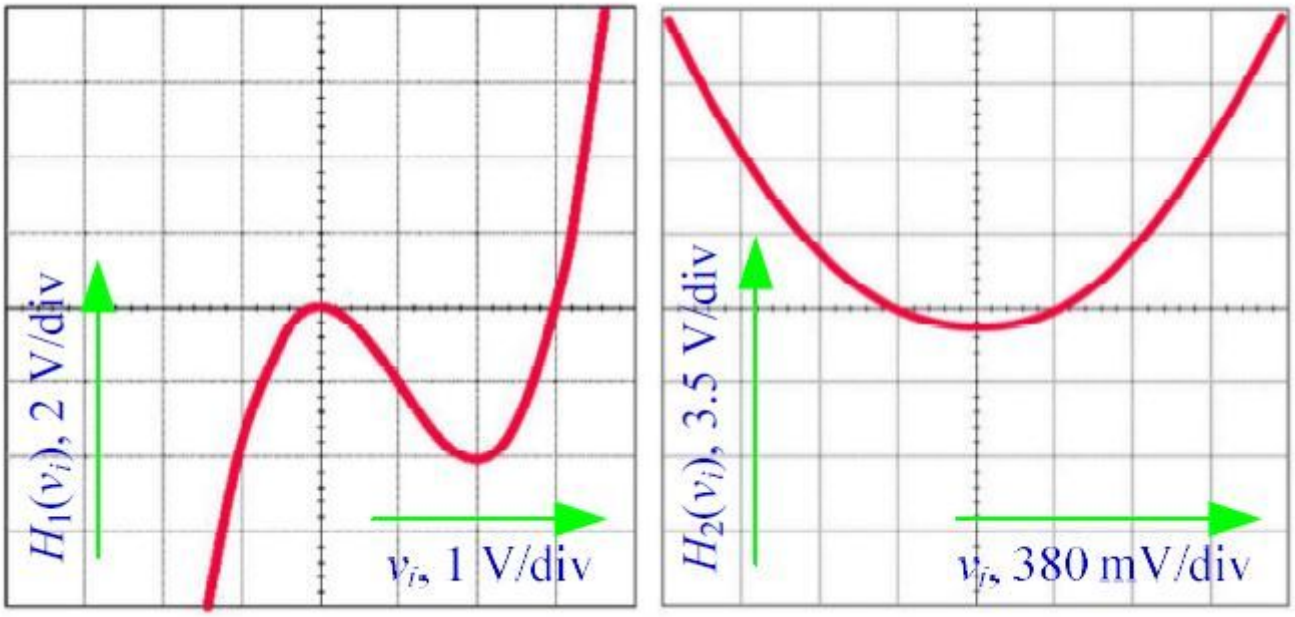

Figure 9

The experimentally measured transfer characteristic curves in the vi – vo voltage plane for the two circuit modules H1(vi) and H2(vi).

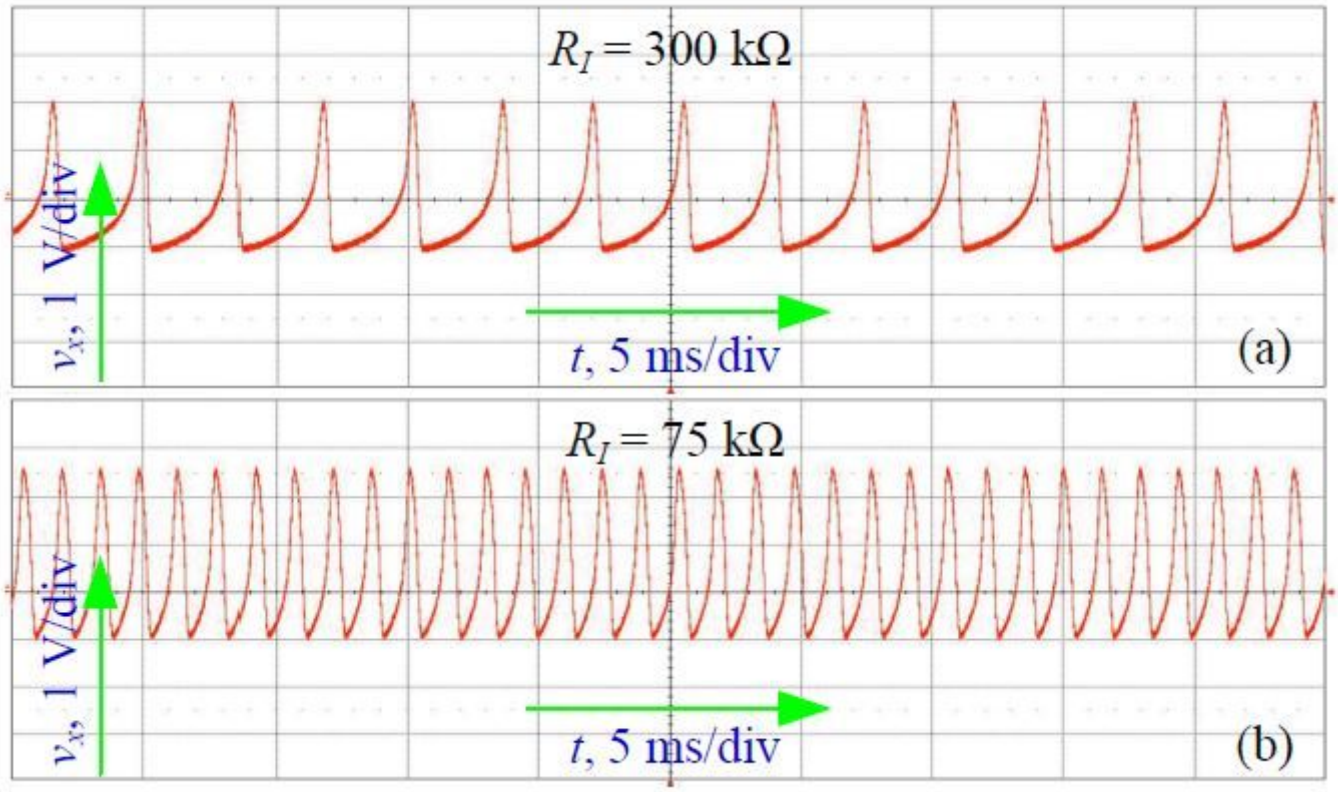

Figure 10

The experimentally measured spiking patterns in the fitted 2D HR neuron model for two representative values of RI. a RI = 300 kΩ and b RI = 75 kΩ.

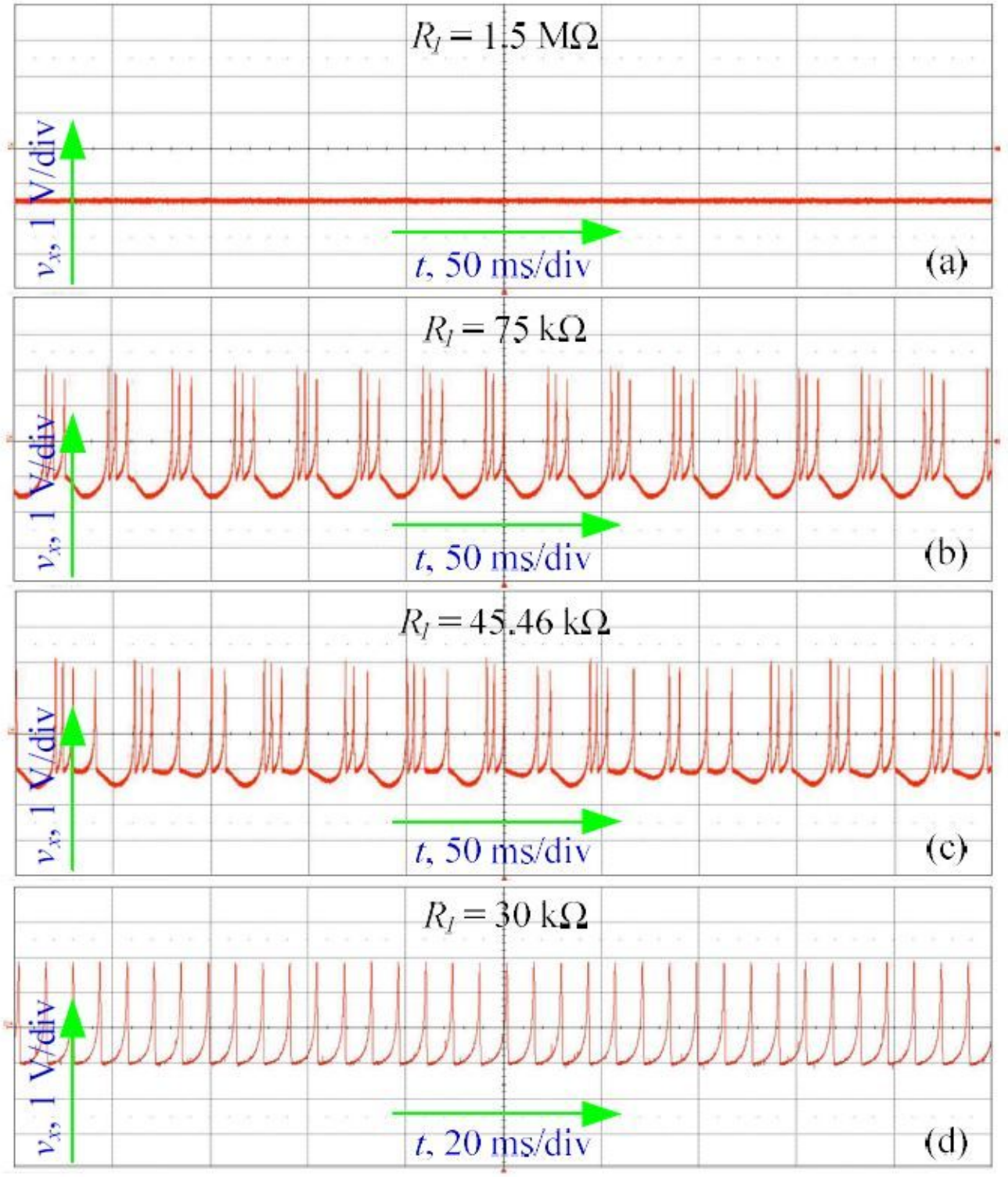

Figure 11

The experimentally measured operation patterns in the fitted 3D HR neuron model for four representative values of RI. a Resting at RI = 1.5 MΩ, b periodic bursting at RI = 75 kΩ, c chaotic bursting at RI = 45.46 kΩ, and d periodic spiking at RI = 30 kΩ.